Journal of Chromatography A, 1216 (2009) 941–947

Contents lists available at ScienceDirect

Journal of Chromatography A

journal homepage: www.elsevier.com/locate/chroma

Characterization of pore structure of a strong anion-exchange membrane adsorbent under different buffer and salt concentration conditions

Ivana Tatárová[a], René Fáber[b], Renaud Denoyel[c], Milan Polakovič[a,*]

[a] Department of Chemical and Biochemical Engineering, Institute of Chemical and Environmental Engineering, Faculty of Chemical and Food Technology, Slovak University of Technology, Radlinského 9, SK-812 37 Bratislava, Slovakia
[b] Sartorius Stedim Biotech GmbH, Göttingen, Germany
[c] Universités d'Aix-Marseille I, II et III-CNRS, UMR 6264: Laboratoire Chimie Provence, Equipe Matdiv, Centre Saint Jérôme, F-13397 Marseille Cedex 20, France

ARTICLE INFO

Article history:
Received 24 September 2008
Received in revised form 3 December 2008
Accepted 5 December 2008
Available online 11 December 2008

Keywords:
Membrane chromatography
Membrane adsorbent
Chromatographic ion exchanger
Pore structure
Pore size distribution
Bimodal model
Transport pores
Gel-layer porosity

ABSTRACT

The quantitative characterization of pore structure of Sartobind Q, a strongly basic membrane anion exchanger that is formed by cross-linked cellulose support and a hydrogel layer on its pore surface, was made combining the results obtained by several experimental techniques: liquid impregnation, batch size-exclusion, inverse size-exclusion chromatography, and permeability. Mercury intrusion and nitrogen sorption porosimetry were carried out for a dry cellulose support membrane in order to get additional information for building a model of the bimodal pore structure. The model incorporated the distribution of the total pore volume between transport and gel-layer pores and the partitioning of solutes of different molecular weights was expressed through the cylindrical pore model for the transport pores and random plane model for the gel layer. The effect of composition of liquid phase on the pore structure was investigated in redistilled water, phosphate and Tris–HCl buffers containing up to 1 M NaCl. Evident differences in the bimodal pore structure were observed here when both the specific volume and size of the hydrogel layer pores significantly decreased with the ionic strength of liquid phase.

1. Introduction

Modified macroporous membranes were introduced as stationary phases in liquid chromatography separations in early 1990s [1–6]. Since then, extensive research has been performed in the field of material and separation design leading to enhancement of the process performance and successful adoption of membrane chromatography in numerous analytical and process-scale applications. Ion-exchange membrane chromatography has become the most successful application type of the technique [7,8]. The main advantage of the separations employing membrane adsorbents is that diffusional limitations typical for low-pressure particle chromatography (especially of macromolecules), which decrease the column resolution with the flow rate, are eliminated.

Owing to large pore sizes of membrane adsorbents, the transport of separated molecules is predominantly due to convective flow, which safeguards high separation efficiency also at elevated flow rates. The continuous character of membrane layer enables a simple scale-up and also operation in a low-pressure range due to a relatively short effective thickness of the layer. The breakthrough capacities of ion-exchange membranes operated at low loads are often comparable to those of commonly used resins [7–10]. Similar values of the resolution have also been achieved [8,11].

The described properties of functionalized membranes make them ideal for purification applications such as the removal of trace impurities or potential contaminants (DNA, viruses or endotoxins) and for separation of sensitive biomolecules (blood factors, monoclonal antibodies, technical enzymes) where a rapid operation decreases the probability of their degradation [9,12]. Moreover, they are very useful in the separation of large protein molecules with the weight-average molecular weight $M_W > 250$ kDa [13].

The most important determinants of overall separation performance and economics are process conditions and structural properties of chromatographic adsorbents [10,14–23]. They determine the rate of the transport to the adsorbent active sites and thus their number available for separation. The structural properties of chromatographic adsorbents can be investigated by several methods. Since many chromatographic adsorbents are based on cross-linked gels or macroporous resins, their porous structure collapses during treatment used in the conventional techniques such as mercury or liquid nitrogen adsorption porosimetry. Moreover, special attention should be kept to the changes in their morphology with the composition of the liquid phase contained inside

* Corresponding author.
E-mail address: milan.polakovic@stuba.sk (M. Polakovič).

0021-9673/$ – see front matter © 2008 Elsevier B.V. All rights reserved.
doi:10.1016/j.chroma.2008.12.018

pores which was also reported for a cation-exchange membrane adsorbent [8]. For these reasons, size-exclusion techniques that are applied to adsorbents in wet state are most commonly used [14,24–32]. Another technique that was applied to the investigation of structural characterization of both porous particle and membrane adsorbents is confocal microscopy combined with fluorescent protein labeling [23]. Using this technique, it is possible to visualize the protein adsorption to ion exchangers in situ.

Size-exclusion data are often interpreted through structural models [25,30–33]. The models are distinguished mainly by the geometry of pores and form of the pore size distribution function. Applying a statistical mechanics approach, Giddings et al. [34] derived equations for the calculation of pore distribution coefficient of spherical molecules in pores of slit, cylindrical and spherical shapes. The particle distribution coefficient was then obtained by the integration of the pore distribution coefficient through the pore size distribution function, mostly represented by the log-normal distribution [27]. For the same three pore geometries, Cassasa [35,36] derived relationships for the calculation of the distribution coefficients of flexible linear and branched macromolecules using random-flight statistics. Jeřábek [37] considered a set of finite number of discrete fractions of pore sizes instead of a continuous distribution function. Grimes et al. [31] assumed separate distribution functions of solute molecules in macropores and mesopores, respectively. Their model could predict the existence of the second inflection point in size-exclusion curves. It was shown in our previous paper that it is difficult to get a credible parameters of a distribution function because many size-exclusion data can be fitted closely with a simple monodisperse model [32].

Several models do not use a pore concept for the characterization of the accessibility of particle structure to solute molecules. Gel structure was described either as a random network of straight fibres of infinite length [38,39] or as a network of surfaces of negligible thickness of random location and orientation [34,40]. Spaces of different sizes between the fibres or surfaces resulted in different obstruction effects for molecules of different molecular weight. Both particle accessibility concepts can be applied to non-spherical solute molecules, if the mean molecule length is used as a characteristic dimension. These models have been successfully applied in our previous studies for the characterization of accessibility of gel materials used for separation of proteins [30,32,41].

The main objective of the study was the quantitative characterization of pore structure of a strongly basic anion exchanger Sartobind Q under different buffer and salt concentration conditions. For that purpose, several types of experiments were carried out for a cellulose support and Sartobind Q membranes: liquid impregnation, batch and chromatographic size-exclusion, mercury and liquid nitrogen porosimetry and permeability. Combining all these results, a consistent description of the bimodal porous structure with a swelling/shrinking hydrogel layer at the pore walls was obtained. A simple model was designed that could predict the accessibility of the membrane adsorbent to molecules of broad sizes very well.

2. Experimental

2.1. Solutes

Glucose and sucrose (Sigma, St. Louis, MO, USA), and dextrans (Fluka BioChemika, Buchs, Switzerland and Sigma) with the weight-average molecular weights 1200, 6000, 9300, 17,500, 40,000, 56,000, 70,000, 110,000, 220,000, 500,000 and 2,000,000 were used as solute probes [26,40,42]. Their hydrodynamic radius, r_s, was calculated from the Mark-Houwink-Sakurada equation [26,27]

$$r_s = 0.027 M_w^{0.5} \quad (1)$$

Table 1
Liquid phases used in size-exclusion and permeability experiments.

Liquid phase[a]	Ionic strength [mol l^{-1}]	Code
Redistilled water	0.002	W0
0.15 M NaCl in redistilled water	0.160	W1
1 M NaCl in redistilled water	1.008	W2
10 mM phosphate buffer, pH 7.0	0.028	P0
0.15 M NaCl in 10 mM phosphate buffer, pH 7.0	0.158	P1
1 M NaCl in 10 mM phosphate buffer, pH 7.0	1.010	P2
15 mM Tris–HCl buffer, pH 7.2	0.022	T0
0.15 M NaCl in 15 mM Tris–HCl buffer, pH 7.2	0.155	T1
1 M NaCl in 15 mM Tris–HCl buffer, pH 7.2	1.013	T2

[a] Sodium azide concentration of 2 mM was applied in order to prevent microbial growth.

5 g l^{-1} solutions of the compounds in liquid phases listed in Table 1 were prepared, filtered through a 0.2 μm filter and stored in refridgerator.

2.2. Adsorbents

Sartobind Q membrane is a strongly basic anion exchanger that is formed by macroporous cross-linked cellulose supported by non-woven and a hydrogel layer at its pore surface. The hydrogel layer carries positively charged quaternary ammonium functional groups and provides an adequate surface area for adsorption of solutes. The thickness of a dry Sartobind Q membrane sheet with glycerol-filled pores was measured using a contact thickness gauge from MTS Systems (Cary, NC, USA). It was found to be 250 μm.

2.3. Liquid impregnation method (LIM)

For the determination of the total specific volume of pores, v_p, a small portion of the membrane was equilibrated with a liquid phase (Table 1) and dried at 60 °C. v_p was calculated as follows:

$$v_p = \frac{1}{m_{ad}} \frac{m_{aw} - m_{ad} + m_s}{\rho_b} \quad (2)$$

$$m_s = (m_{aw} - m_{ad}) \frac{\sum_i c_{s,i}}{\rho_b - \sum_i c_{s,i}} \quad (3)$$

where m_{aw} and m_{ad} are the masses of wet and dry membranes, respectively, m_s is the mass of salts corresponding to the amount of evaporated water, $m_{aw} - m_{ad}$, ρ_b is the liquid phase density and $c_{s,i}$ is the concentration of i-th salt contained in the liquid phase. Due to a relatively small concentration of other salts, only the sodium chloride contribution to the solution density was considered.

The porosity of the membranes was calculated as the ratio of v_p, and specific membrane volume, v_m, as follows:

$$\varepsilon_p = \frac{v_p}{v_m} = \frac{v_p}{v_p + v_{ds}} = \frac{v_p}{v_p + \frac{1}{\rho_{ds}}} \quad (4)$$

where v_{ds} is the volume of dry solid membrane fraction and ρ_{ds} is its density, which was determined by mercury porosimetry to be 1.43 g cm^{-3}.

2.4. Size-exclusion experiments

2.4.1. Batch size-exclusion method (BSEM)

Membrane samples were first properly washed with redistilled water. Glycerol contained in Sartobind Q membrane was thus completely removed. The samples were then equilibrated with a liquid phase (Table 1) using three successive rinsing steps with a high excess of flushing liquid that were evenly distributed during 24 h. Afterwards, the liquid adhered to the membrane outer surface was removed so that the membrane was inserted between two paper

sheets and pressed by hand. The membrane samples were then cut into pieces of the size of approximately 5 mm × 5 mm and put into flasks together with predefined amounts of probe solutions. The flasks were sealed and stirred on a reciprocal shaker for at least 80 h. The samples were then separated by filtration. The experiments were realized in triplicates for all solute/liquid phase combinations.

The equilibrium concentration of dextran solutions was determined by differential refractometer of a chromatography set-up from Knauer (Berlin, Germany). If the solution contained sodium chloride, this was separated on a SEC column inserted between the injection sampling port and RI detector (Biosep, Phenomenex, Torrance, CA, USA). The equilibrium concentration of glucose solutions was determined using a colorimetric method employing an enzymatic reaction (GLU GOD BIO-LA-Test, PLIVA-Lachema Diagnostika, Brno, Czech Republic). The specific volume of pores accessible to a solute, v_d, was calculated from the following equation:

$$v_d = \left(\frac{c_m^0}{c_m^{eq}} - 1 \right) \frac{V_s}{m_{ad}} \quad (5)$$

where c_m^0 and c_m^{eq} are the solute initial and equilibrium concentrations, respectively, and V_s is the volume of probe solution contacted with a membrane sample.

The specific pore volume accessible to the largest dextran (hydrodynamic radius of 38 nm), $v_{d,min}$, was used to distribute the total specific pore volume, v_p, between two fractions. The accessible fraction defined the specific volume of transport pores, v_T, the pore volume fraction inaccessible to this solute represented the specific volume of either gel-layer, v_G, or cellulose network pores, v_C.

2.4.2. Inverse size-exclusion chromatography (ISEC)

Chromatographic experiments were realized either in the column Pharmacia HR 5/5 packed with support membrane pieces using a packing procedure recommended by the supplier (50 mm × 5 mm I.D., Amersham Biosciences, Uppsala, Sweden) or in a Sartobind Q membrane module MA 75 (15 membrane layers, 5 cm^2 frontal area). Both the column and module were first equilibrated with a liquid phase (Table 1). Solute samples were then injected and the concentration at the column outlet was recorded by the means of differential refractometer (Knauer).

The solute retention time in the chromatographic system, t_R, and corresponding retention volume, V_R, were calculated from the first absolute moment of the residence time distribution function obtained from the chromatographic signal. The V_R-values were used to calculate the specific pore volumes accessible to individual solutes in the following way:

$$v_d = v_{d,min} + \frac{V_R - V_{R,min}}{V_{R,max} - V_{R,min}} (v_{d,max} - v_{d,min}) \quad (6)$$

$v_{d,min}$ and $v_{d,max}$ are the specific pore volumes accessible to the largest dextran and glucose, respectively, determined by BSEM and $V_{R,min}$ and $V_{R,max}$ are their corresponding retention volumes obtained by ISEC.

2.5. Measurement of permeability

Membrane discs (d = 47 mm) were properly washed with redistilled water and contacted with a 1 M NaCl solution for at least 15 min. After further washing, the samples were equilibrated with a liquid phase (Table 1) and one by one put between a formed plate and sealing ring of a cylindrically-shaped apparatus for permeability measurement (Sartorius, Goettingen, Germany). Approximately 100 ml of the corresponding liquid phase solution was poured into the cylinder, while the bottom part was sealed. The solution flux was determined by recording the solution volume, V, transferred through a membrane area, A, per time, t, at a pressure difference, Δp. The permeability, P, was then calculated as follows:

$$P = \frac{V}{\Delta p A t} \quad (7)$$

The apparent mean pore radius was estimated using the Hagen-Poiseuille's equation,

$$r_{p,app} = \sqrt{P \frac{8 \mu z}{\varepsilon_p} \tau} \quad (8)$$

where μ is the liquid phase dynamic viscosity, ε_p the membrane porosity, z the membrane thickness and τ the membrane tortuosity, which was determined by a conductivity method [43].

2.6. Mercury intrusion porosimetry (Hg-P)

Mercury intrusion porosimetry measurements were carried out using a Porosimeter 2000 from Fisons Instruments (San Carlos, CA, USA). The estimation of pore diameter from the applied pressure was based on the Washburn equation. The surface tension of mercury was considered to be of 4.8×10^{-3} N/cm, while the value of mercury contact angle of 141° was used. The information provided by Hg-P software included pore size distribution, specific pore volume and dry solid membrane density. A cumulative surface area in a given pore range was calculated from the Rootare–Prenzlow equation [44].

2.7. Nitrogen adsorption technique (N_2-A)

The nitrogen adsorption-desorption isotherms at 77 K were determined by a Micrometrics (Norcross, CA, USA) ASAP 2010 apparatus. Before adsorption experiment, samples were evacuated at 100 °C under a residual pressure lower than 10^{-3} Pa. Depending on the measured adsorption isotherm type, surface area and pore size distribution can be deduced from N_2-A technique. The BET equation was applied to determine the surface area.

3. Results and discussion

Sartobind Q is a commercial anion-exchange membrane adsorbent formed by a macroporous support based on reinforced cross-linked cellulose containing a hydrogel layer on the macropore walls (Fig. 1). The presence of the hydrogel layer decreases the cross-section area and volume of convective transport pores compared to the support membrane. Simultaneously, it provides a fraction of porous structure with bound ion-exchange ligands and high specific surface area where separation takes place. In order to obtain a consistent, quantitative picture about this bimodal texture, a combination of LIM, BSEM, ISEC, permeability, Hg-P, and N_2-A measurements was employed.

3.1. Basic characterization of porosity

The support membrane was characterized by all six techniques mentioned above whereas N_2-A measurement was not realized for Sartobind Q membrane. The total specific pore volume, v_p, in redistilled water (W0) was determined by the LIM and was found to be 2.44 ml g^{-1} for the support membrane and 2.40 ml g^{-1} for Sartobind Q. Using these v_p-values, the specific membrane volume, v_m, of both membranes was calculated from Eq. (4) to be 3.13 ml g^{-1} and 3.09 ml g^{-1}, respectively, which corresponded well with the values 3.18 ml g^{-1} and 3.14 ml g^{-1}, respectively, obtained from the membrane geometry (frontal area and thickness, Section 2.2). The density of membrane bed, which is an inverse value of the specific membrane volume, was 0.319 g ml^{-1} and 0.324 g ml^{-1}, respectively. Consequently, the porosity, ε_p, (Eq. (4)) was also about the same

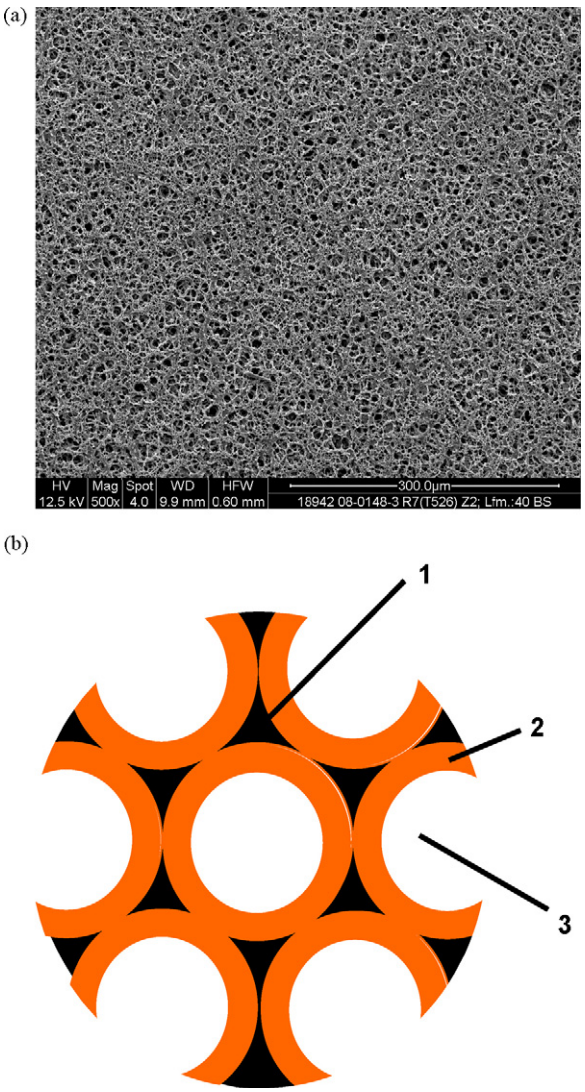

Fig. 1. Structure of Sartobind Q membrane: (a) scanning electron micrograph, (b) scheme of the structure (1: cellulose support, 2: hydrogel layer, 3: transport pores).

for both membranes–0.780 and 0.777, respectively. Based on these results, it could be concluded that no swelling of the support membrane occurred in wet state.

Fig. 2a and b depict dependences of the specific accessible pore volume, v_d, on the solute hydrodynamic radius, r_s, obtained by BSEM/ISEC in W0 for the support and Sartobind Q membranes, respectively. As was described in Section 2.4, the specific pore volume accessible to the largest solute, $v_{d,min}$, allowed us to calculate the specific volumes of transport pores, v_T, hydrated cellulose network pores in the support membrane, v_C, and hydrogel layer pores in Sartobind Q, v_G (Table 2). The values of v_C and v_G were 0.50 ml g^{-1} and 0.82 ml g^{-1}, respectively. The specific volume of transport pores was thus larger in the support membrane than in Sartobind Q; 1.95 ml g^{-1} compared to 1.55 ml g^{-1}.

The presence of the gel layer thus decreases the specific volume of transport pores of Sartobind Q and these are definitely narrower than those of the support membrane. This was confirmed by the permeability measurements (Table 3) where a much lower resistance to the solution flow and thus a significantly higher permeability value, P, of 655 ml min^{-1} bar^{-1} cm^{-2} was measured for the support membrane. For Sartobind Q, the observed value of P was only 149 ml min^{-1} bar^{-1} cm^{-2}. Using the Hagen-Poiseuille's equation (Eq. (8)), the apparent mean pore radius, $r_{p,app}$, was calculated

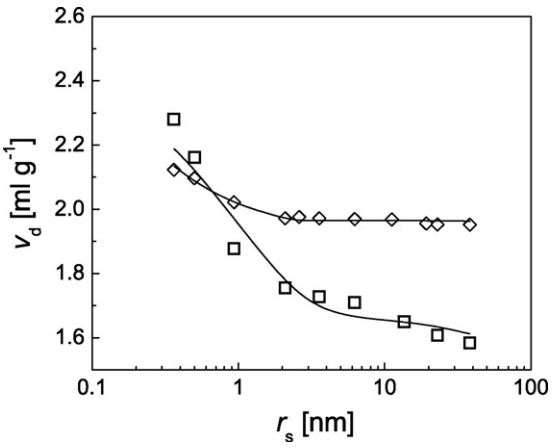

Fig. 2. Specific accessible pore volume vs. solute hydrodynamic radius dependence for support membrane (diamonds) and Sartobind Q membrane (squares) in redistilled water obtained by BSEM/ISEC.

for the total porosity ($\varepsilon_p = 0.78$) and tortuosity ($\tau = 1.64$). It was found to be equal to 2.0 µm for the support membrane and 0.9 µm for Sartobind Q. The difference is in principle in agreement with the interpretation of the Hagen-Poiseuille's equation for the flow through polydisperse materials that larger pores contribute more significantly to the permeability.

Fig. 2a further shows that v_d for the support membrane decreased quickly with the solute hydrodynamic radius from the highest value of about 2.1 ml g^{-1} for glucose down to a practically constant value of 1.95 ml g^{-1} for solutes having r_s larger than 2 nm. This implies that size-exclusion effect in the transport pores of the support membrane was negligible. It also indicates that the radius of the transport pores could be larger than 1 µm. A similar fast

Table 2
Specific pore volume of examined membranes determined by BSEM technique in different liquid phases.

Membrane	Liquid phase	Pore volume [ml g^{-1}]			
		v_p	v_C	v_G	v_T
Support	W0	2.44 ± 0.03	0.49	–	1.95
	W1	2.44 ± 0.03	0.41	–	2.03
	W2	2.44 ± 0.03	0.52	–	1.93
Sartobind Q	W0	2.40 ± 0.01	–	0.82	1.58
	W1	2.43 ± 0.02	–	0.51	1.92
	W2	2.50 ± 0.09	–	0.53	1.98
	P0	2.38 ± 0.01	–	0.76	1.62
	P1	2.43 ± 0.05	–	0.85	1.60
	P2	2.46 ± 0.01	–	0.51	1.94
	T0	2.41 ± 0.04	–	0.82	1.59
	T1	2.45 ± 0.02	–	0.59	1.96
	T2	2.55 ± 0.03	–	0.58	1.96

Table 3
Permeability and apparent mean pore radii of the support and Sartobind Q membranes in different liquid phases.

Membrane	Liquid phase	P [ml min^{-1} bar^{-1} cm^{-2}]	$r_{p,app}$ [µm]
Support	W0	654.7 ± 18.2	2.01
Sartobind Q	W0	149.0 ± 0.0	0.92
	W1	386.0 ± 7.8	1.49
	W2	417.1 ± 19.3	1.62
	P0	336.3 ± 6.5	1.38
	P1	308.1 ± 13.3	1.33
	P2	381.2 ± 14.8	1.55
	T0	256.3 ± 0.1	1.21
	T1	307.4 ± 13.4	1.33
	T2	305.2 ± 3.2	1.39

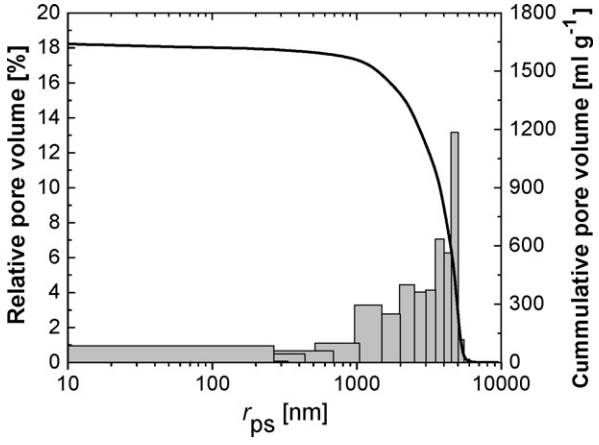

Fig. 3. Pore volume distribution of support membrane determined by Hg-P technique.

decrease in sub-nanometer solute size was observed for Sartobind Q as well but ν_d decreased here gradually in the whole examined r_s-range up to 40 nm (Fig. 2b). This is an evidence of a presence of cross-linked swollen network with a typical wide distribution of openings (pores) provided by the gel layer on the membrane surface.

It should be further noticed from the data in Table 2 and Fig. 2 that the inaccessible specific volume for glucose was about 0.3 ml g^{-1} in the support membrane but only 0.1 ml g^{-1} in Sartobind Q. This can be explained by that the preparation procedure of Sartobind Q from the support membrane opened up domains in the cellulose matrix and these were filled with the swollen grafted polymer. Only a smaller part of the total pore volume became then inaccessible for glucose. This observation substantiates the above-made assignment of ν_G to the specific pore volume of the gel layer. The gel-layer pores thus formed one third of the total pore volume of Sartobind Q membrane.

A very approximate estimate of the range of pore sizes of the gel layer could be obtained from the corresponding sizes of solute molecules partially excluded from these pores. For polysaccharide standards, a 2.5–3-multiple of their size is considered as a good approximation of pore size [41]. Applying this rule of thumb, the radius of most pores of the hydrogel layer of Sartobind Q membrane could be smaller than 10 nm. The continuous decrease of ν_d with r_s even at the solute radii of 10–40 nm indicates that these solutes could be slightly excluded from smaller transport pores of Sartobind Q.

Hg-P technique gave the values of specific pore volumes of 1.60 ml g^{-1} for the support membrane and 1.34 ml g^{-1} for Sartobind Q. These values were slightly lower than the values of ν_T determined by BSEM (Table 2). The differences can be most likely assigned to a compression of the membranes at high pressures applied and/or pore volume lowering by the shielding effect of small pores [45]. The value obtained for Sartobind Q also confirms expected collapse of the gel layer by drying during sample preparation. A similar pore volume distribution and mean pore radius of 4.7 μm was observed for both membranes. Fig. 3 illustrates for the support membrane that most pore were in the r_s-range of 1–7 μm. Naturally, similar values of the surface area, a, were calculated from the distribution data: 1.05 m^2 g^{-1} for the support membrane and 0.98 m^2 g^{-1} for Sartobind Q. The surface area calculation was limited to pores larger than 1 μm because high pressures corresponding to smaller pore radii could induce a high error due to the compression of the materials.

The mean pore radius of the support membrane determined by Hg-P is more than twice larger than the $r_{p,app}$-value obtained from the permeability measurement. It should be underscored here that we consider the former value as more reliable. The ratio of the membrane thickness to the pore radius is relatively low so a fully developed laminar flow, needed for the validity of the Hagen-Poiseuille's equation, will not occur over the longer part of the axial distance of the membrane. More importantly, the 'fishermen net-like' structure of the membrane is very distant from a system of parallel cylindrical pores implicitly assumed in the calculation. Numerous changes of flow cross-section area would result in additional local pressure drops that effectively decrease the value of apparent radius.

The adsorption–desorption isotherm of nitrogen on the support membrane was of type II according to the IUPAC classification. It means that the pores are too large to be analyzed by a method for determination of pore volume and pore size distribution. Only the BET specific surface area could be calculated. The value was 0.90 m^2 g^{-1}, which is in a reasonable agreement with the result of Hg-P measurement.

3.2. Effect of ionic strength

A detailed study of the effect of ionic strength on the membrane structure was performed at three different concentrations of sodium chloride—0 M, 0.15 M and 1 M, and two buffers typically used in anion-exchange separations using the LIM, BSEM, ISEC and permeability measurements. Table 2 shows that ν_p as well as the ratio of ν_C and ν_T of the support membrane in W0 was practically the same for the three ionic strengths tested. For Sartobind Q, the ν_p-values at zero salt concentration were approximately 2.4 ml g^{-1} in all types of liquid phases. A slight increase of the total specific pore volume with ionic strength was observed in all solutions when the highest difference of 6% was observed in the Tris–HCl buffer containing 1 M sodium chloride.

A significant change in the distribution of total pore volume between the transport and gel-layer of Sartobind Q was found with the variation of the ionic strength (Table 2). At zero NaCl concentration, ν_T had a value of approximately 1.60 ml g^{-1} for all three types of liquid phases. An approximately the same value of 1.95 ml g^{-1} was obtained for 1 M NaCl solutions. In the two cases (W1, T1), the sodium chloride concentration of 0.15 M represented a sufficient ionic strength to approach a value of 1.90 ml g^{-1}. On the contrary, no significant difference in the membrane structure compared to salt-free conditions was observed in P1. The values of ν_G were in the range of 0.76–0.82 ml g^{-1} at zero NaCl concentration. They decreased to 0.51–0.59 ml g^{-1} at all liquid phases with a higher ionic strength besides P1. The shrinkage of the volume of gel layer with ionic strength from about 35% to 20% of the total pore volume was thus in agreement with previously reported results for Sartobind S membrane [8]. The differences in the swelling/shrinking behaviour in phosphate and Tris–HCl buffers are nicely illustrated on the dependencies of accessible specific pore volume vs. hydrodynamic solute radius obtained from BSEM/ISEC experiments (Fig. 4a and b). The boundary points of the lines are identical with the values in Table 2. The curves thus illustrate the width of pore size distribution. In the absence of salt, ν_d was decreasing significantly for the solutes having the hydrodynamic radius smaller than 10 nm but it was decreasing in a much lower range for 1 M NaCl. This corresponds to a significant decrease of openings in the polymer network forming the gel layer (T2 in Fig. 3b).

The permeability measurements presented in Table 3 confirmed the effect of ionic strength on the swelling/shrinking behaviour of the gel layer of Sartobind Q. The P-values corresponded well with the ν_T determined by BSEM experiments, when the effect of ionic strength was analyzed separately for each solution type (Tables 2 and 3). In distinction to ν_T, the permeability differed for the liquid phases not containing NaCl. The smallest P-value

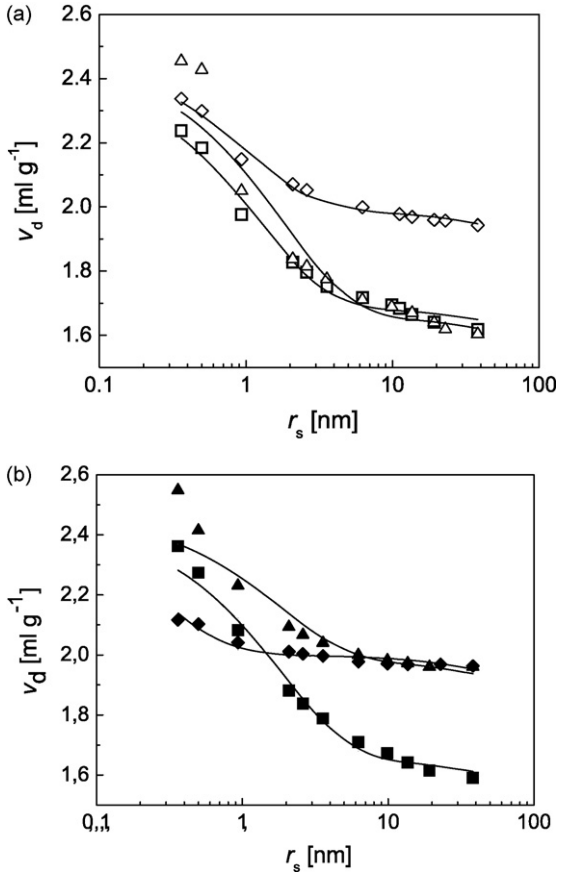

Fig. 4. Specific accessible pore volume vs. solute hydrodynamic radius dependence for Sartobind Q membrane obtained by BSEM/ISEC in the following liquid phases: (a) P0 (open squares), P1 (open triangles) and P2 (open diamonds); (b) T0 (closed squares), T1 (closed triangles), and T2 (closed diamonds). Lines represent the fits with the model (Eqs. (9)–(11)).

of 149 ml min^{-1} bar^{-1} cm^{-2} was obtained in W0 whereas values equal to 256 ml min^{-1} bar^{-1} cm^{-2} and 336 ml min^{-1} bar^{-1} cm^{-2} were measured in T0 and P0, respectively.

The permeability increased with ionic strength when it was much more pronounced in water than in the buffers. At the sodium chloride concentration of 1 M, the factor of increase compared to the zero NaCl concentration was 2.8-times for water but only about 1.2-times for the buffers. Of course, an analogous trend could be observed in the values of $r_{p,app}$ calculated from P using the Hagen-Poiseuille's equation (Eq. (8)). The apparent transport pore radius of Sartobind Q in W0 was 0.92 μm whereas in other liquid phases, it was from 1.21 μm to 1.62 μm. As has been explained above, the true values of transport pore radius will be higher due to a significant deviation of porous structure from cylindrical pores.

3.3. Modelling of pore structure

Two types of model approaches discussed in Introduction were combined in order to get a consistent model of the bimodal structure of the membranes that could provide a close fit of the experimental v_d vs. r_s curves presented in Figs. 2 and 4. The random plane model of Giddings was applied to the characterization of the texture of the hydrogel layer of Sartobind Q and cellulose structure network of the support membrane. A model of cylindrical pores was considered to describe the partitioning of solutes in the transport pores. The accessible volume of a solute was thus obtained as a sum

Table 4
Parameters of the bimodal model of membrane structure (Eqs. (9)–(11)) and their standard deviations.

Membrane	Liquid phase	s [m^2 ml^{-1}]	v_T [ml g^{-1}]	SD [%]
Support	W0	3310 ± 120	2.00 ± 0.01	1.3
Sartobind Q	W0	942 ± 144	1.67 ± 0.03	1.8
	P0	752 ± 52	1.69 ± 0.01	1.2
	P1	529 ± 99	1.66 ± 0.04	2.6
	P2	917 ± 62	1.99 ± 0.01	1.1
	T0	512 ± 44	1.66 ± 0.02	1.2
	T1	525 ± 135	1.99 ± 0.03	2.8
	T2	3790 ± 280	2.00 ± 0.01	2.3

SD: relative standard deviation of v_d.

of two terms:

$$v_d = (v_p - v_T)\exp(-sr_s) + v_T K_p \quad (9)$$

where s is the specific surface area per unit volume and $v_p - v_T$, the specific pore volume of gel layer or cellulose structure network, respectively. The specific volume of transport pores, v_T, was not assigned here to the accessible volume of largest dextran but it was a fitted parameter because the transport pore partition coefficient, K_p, could have values lower than one. A simple form of the cylindrical pore model was used for Sartobind Q to calculate K_p,

$$K_p = \left(1 - \frac{r_s}{r_p}\right)^2 \quad (10)$$

A single value of pore radius r_p was obtained by multiplying the value of $r_{p,app}$ determined by the permeability measurements (Table 3) with the factor of 2 (the ratio of true and apparent pore radii found for the support membrane; Section 3.1). For the support membrane, K_p was obtained by summing through the pore size distribution obtained by Hg-P,

$$K_p = \sum_i f_i \left(1 - \frac{r_s}{r_{pi}}\right)^2 \quad (11)$$

where, r_{pi} is the pore radius and f_i the volumetric fraction of the i-th size fraction of the transport pores.

The fitted curves and estimated parameters of the model are presented in Figs. 2 and 4 and Table 4, respectively. Generally, the model provided a very good characterization of the accessibility of both membranes and reliable description of the bimodal structure of the membranes. The relative standard deviations of v_d were typically smaller than 2% with the exceptions of the cases where small discrepancies between the v_d-values for the smallest solute probes determined by BSEM and v_p-values determined by LIM (Fig. 4 and Table 2) were observed. The fitted v_T-values (Table 4) were by 2–5% larger compared to those estimated by BSEM (Table 2). This difference corresponded to the expected small exclusion of large solutes from the transport pores that was incorporated into the bimodal model.

Table 4 also shows that the values of v_T were predicted with a very good accuracy. The uncertainties, represented by the standard deviations, of the second estimated parameter of the model-specific surface area per membrane volume, s, were somewhat higher but still very good. Since s is proportional to the density of polymer network, its reciprocal value corresponds to the characteristic pore dimension. It is therefore not surprising that the largest values of s more than 3000 m^2 ml^{-1}, were obtained for the support membrane and Sartobind Q in 1 M NaCl Tris–HCl buffer, when the ranges of both r_s and v_d of small/medium-sized pores were narrow and their values low (Figs. 2 and 3b). In cases of a more swollen gel layer, the s-values were between 500 m^2 ml^{-1} and 900 m^2 ml^{-1} and pore size distribution of the gel layer was wider (Figs. 2 and 4).

4. Conclusions

The principal contribution of this investigation is that a complete quantitative characterization of bimodal porous structure of a membrane-based chromatographic adsorbent was achieved combining different experimental techniques. This task was simplified by that the dimensions of the two types of pores are very different with relatively narrow pore size distributions each. The transport pores of Sartobind Q are of micrometer size whereas the pores of the swollen gel network are of nanometer size. The size-exclusion solute probes used could then fully access the volume of transport pores while they showed a complete spectrum of performance from full accessibility to complete exclusion in the gel-layer pores.

A very good estimate of the volume of transport pores could then be obtained from the accessible volume of the largest solute probe determined by the batch size-exclusion method. Inverse size-exclusion chromatography provided the values of partition coefficients for the set of solute probes that could be transformed into accessible volumes using only two experimentally determined values of the accessible volume—for glucose and largest dextran. This good mapping of the accessibility of gel-layer pores became the basis for a bimodal model of pore structure of Sartobind Q membrane that could predict the overall accessibility for molecules of different size. Additional useful information about the structure of transport pores was obtained from the mercury porosimetry and permeability measurements. The developed method was successfully applied to the quantification of the effect of ionic strength on the pore structure. All these results can become valuable at the optimization of membrane adsorbents aimed at their optimal performance in separation of biomolecules.

Acknowledgement

This study was supported by a grant of the Slovak Grant Agency for Science VEGA (Grant No. 1/3565/06).

References

[1] R. Molinari, J.L. Torres, A.S. Michaels, P.K. Kilpatrick, R.G. Carbonell, Biotechnol. Bioeng. 36 (1990) 572.
[2] T.B. Tennikova, B.G. Belenkii, F. Svec, J. Liq. Chromatogr. 13 (1990) 63.
[3] P. Langlotz, K.H. Kroner, J. Chromatogr. 591 (1992) 107.
[4] S.Y. Suen, M. Caracotsios, M.R. Etzel, Chem. Eng. Sci. 48 (1993) 1801.
[5] E. Klein, E. Eichholz, F. Theimer, D. Yeager, J. Membr. Sci. 95 (1994) 199.
[6] A. Shiosaki, M. Goto, T. Hirose, J. Chromatogr. A 679 (1994) 1.
[7] N. Kubota, S. Miura, K. Saito, K. Sugita, K. Watanabe, T. Sugo, J. Membr. Sci. 117 (1996) 135.
[8] K.H. Gebauer, J. Thommes, M.R. Kula, Chem. Eng. Sci. 52 (1997) 405.
[9] J.X. Zhou, T. Tressel, U. Gottschalk, F. Solamo, A. Pastor, S. Dermawan, T. Hong, O. Reif, J. Mora, F. Hutchison, M. Murphy, J. Chromatogr. A 1134 (2006) 66.
[10] J.X. Zhou, T. Tressel, Bioprocess Int. 3 (2005) 32.
[11] M.B. Tennikov, N.V. Gazdina, T.B. Tennikova, F. Svec, J. Chromatogr. A 798 (1998) 55.
[12] H.L. Knudsen, R.L. Fahrner, Y. Xu, L.A. Norling, G.S. Blank, J. Chromatogr. A 907 (2001) 145.
[13] H.N. Endres, J.A. Johnson, C.A. Ross, J.K. Welp, M.R. Etzel, Biotechnol. Appl. Biochem. 37 (2003) 259.
[14] Y. Yao, A.M. Lenhoff, J. Chromatogr. A 1126 (2006) 107.
[15] A. Katiyar, L. Ji, P. Smirniotis, N.G. Pinto, J. Chromatogr. A 1069 (2005) 119.
[16] J. Hubbuch, T. Linden, E. Knieps, A. Ljunglof, J. Thommes, M.-R. Kula, J. Chromatogr. A 1021 (2003) 93.
[17] V. Kasche, M. de Boer, C. Lazo, M. Gad, J. Chromatogr. B 790 (2003) 115.
[18] U. Reichert, T. Linden, G. Belfort, M.-R. Kula, J. Thommes, J. Membr. Sci. 199 (2002) 161.
[19] E.B. Schirmer, G. Carta, AlChE J. 53 (2007) 1472.
[20] A.K. Hunter, G. Carta, J. Chromatogr. A 897 (2000) 81.
[21] P. DePhillips, A.M. Lenhoff, J. Chromatogr. A 933 (2001) 57.
[22] B.C.S. To, A.M. Lenhoff, J. Chromatogr. A 1141 (2007) 191.
[23] U. Reichert, T. Linden, G. Belfort, M.R. Kula, J. Thömmes, J. Membr. Sci. 199 (2002) 161.
[24] M. Ousalem, X.X. Zhu, J. Hradil, J. Chromatogr. A 903 (2000) 13.
[25] A.P. Broek, H.A. Teunis, D. Bargeman, E.D. Sprengers, H. Strathmann, C.A. Smolders, J. Membr. Sci. 99 (1995) 217.
[26] L. Hagel, M. Ostberg, T. Andersson, J. Chromatogr. A 743 (1996) 33.
[27] P. DePhillips, A.M. Lenhoff, J. Chromatogr. A 883 (2000) 39.
[28] M. Al-Bokari, D. Cherrak, G. Guiochon, J. Chromatogr. A 975 (2002) 275.
[29] D.J. Winzor, J. Biochem. Biophys. Methods 56 (2003) 15.
[30] G. Grznárová, S. Yu, V. Štefuca, M. Polakovič, J. Chromatogr. A 1092 (2005) 107.
[31] B.A. Grimes, R. Skudas, K.K. Unger, D. Lubda, J. Chromatogr. A 1144 (2007) 14.
[32] I. Tatárová, M. Gramblička, M. Antošová, M. Polakovič, J. Chromatogr. A 1193 (2008) 129.
[33] M.A. Kuntz, P.L. Dubin, J.I. Kaplan, M.S. Mehta, J. Phys. Chem. 98 (1994) 7063.
[34] J.C. Giddings, E. Kucera, C.P. Russell, M.N. Myers, J. Phys. Chem. 72 (1968) 4397.
[35] E.F. Casassa, J. Polym. Sci., Part B 5 (1967) 773.
[36] E.F. Casassa, Macromolecules 9 (1976) 182.
[37] K. Jeřábek, Anal. Chem. 57 (1985) 1595.
[38] A.G. Ogston, Trans. Faraday Soc. 54 (1958) 1754.
[39] T.C. Laurent, J. Killander, J. Chromatogr. 14 (1964) 304.
[40] Y. Yao, A.M. Lenhoff, J. Chromatogr. A 1037 (2004) 273.
[41] P. Gemeiner, M. Polakovič, D. Mislovičová, V. Štefuca, J. Chromatogr. B 715 (1998) 245.
[42] P.L. Dubin, Carbohydr. Polym. 25 (1994) 295.
[43] M. Barrande, R. Bouchet, R. Denoyel, Anal. Chem. 79 (2007) 9115.
[44] H.M. Rootare, C.F. Prezlow, J. Phys. Chem. 71 (1967) 2733.
[45] P.A.C. Gane, C.J. Ridgway, E. Lehtinen, R. Valiullin, I. Furo, J. Schoelkopf, H. Paulapuro, J. Daicic, Ind. Eng. Chem. Res. 43 (2004) 7920.